# *Escherichia coli* Biofilms Have an Organized and Complex Extracellular Matrix Structure

**Chia Hung,[a,b,c] Yizhou Zhou,[f] Jerome S. Pinkner,[a,d] Karen W. Dodson,[a,d] Jan R. Crowley,[c] John Heuser,[e] Matthew R. Chapman,[f] Maria Hadjifrangiskou,[g] Jeffrey P. Henderson,[a,b,c,d] Scott J. Hultgren[a,d]**

Center for Women's Infectious Diseases Research,[a] Division of Infectious Diseases,[b] Department of Internal Medicine,[c] Department of Molecular Microbiology,[d] and Department of Cell Biology and Physiology,[e] Washington University School of Medicine, St. Louis, Missouri, USA; Department of Molecular, Cellular and Developmental Biology, University of Michigan, Ann Arbor, Michigan, USA[f]; Department of Pathology, Microbiology & Immunology, Vanderbilt University, Nashville, Tennessee, USA[g]

**ABSTRACT** **Bacterial biofilms are ubiquitous in nature, and their resilience is derived in part from a complex extracellular matrix that can be tailored to meet environmental demands. Although common developmental stages leading to biofilm formation have been described, how the extracellular components are organized to allow three-dimensional biofilm development is not well understood. Here we show that uropathogenic *Escherichia coli* (UPEC) strains produce a biofilm with a highly ordered and complex extracellular matrix (ECM). We used electron microscopy (EM) techniques to image floating biofilms (pellicles) formed by UPEC. EM revealed intricately constructed substructures within the ECM that encase individual, spatially segregated bacteria with a distinctive morphology. Mutational and biochemical analyses of these biofilms confirmed curli as a major matrix component and revealed important roles for cellulose, flagella, and type 1 pili in pellicle integrity and ECM infrastructure. Collectively, the findings of this study elucidated that UPEC pellicles have a highly organized ultrastructure that varies spatially across the multicellular community.**

**IMPORTANCE** **Bacteria can form biofilms in diverse niches, including abiotic surfaces, living cells, and at the air-liquid interface of liquid media. Encasing these cellular communities is a self-produced extracellular matrix (ECM) that can be composed of proteins, polysaccharides, and nucleic acids. The ECM protects biofilm bacteria from environmental insults and also makes the dissolution of biofilms very challenging. As a result, formation of biofilms within humans (during infection) or on industrial material (such as water pipes) has detrimental and costly effects. In order to combat bacterial biofilms, a better understanding of components required for biofilm formation and the ECM is required. This study defined the ECM composition and architecture of floating pellicle biofilms formed by *Escherichia coli*.**

**Received** 7 August 2013 **Accepted** 12 August 2013 **Published** 10 September 2013

**Citation** Hung C, Zhou Y, Pinkner JS, Dodson KW, Crowley JR, Heuser J, Chapman MR, Hadjifrangiskou M, Henderson JP, Hultgren SJ. 2013. *Escherichia coli* biofilms have an organized and complex extracellular matrix structure. mBio 4(5):e00645-13. doi:10.1128/mBio.00645-13.

**Editor** Yves Brun, Indiana University

**Copyright** © 2013 Hung et al. This is an open-access article distributed under the terms of the Creative Commons Attribution-Noncommercial-ShareAlike 3.0 Unported license, which permits unrestricted noncommercial use, distribution, and reproduction in any medium, provided the original author and source are credited.

Address correspondence to Scott J. Hultgren, hultgren@borcim.wustl.edu.

Bacteria within a biofilm are embedded in a dense extracellular matrix (ECM) composed of several macromolecules, including exopolysaccharides, nucleic acids, and proteins (1–6). Both the physical barriers provided by the ECM and the physiologic state of bacteria in the biofilm protect them from predation and antibacterial insults, such as radiation, cations, and desiccation (7–11). In the case of bacterial pathogens, this protection may permit bacteria to resist antibiotics and recur when treatment is suspended (12, 13).

Bacteria are able to produce biofilms in diverse niches, including abiotic surfaces, living cells, and at the air-liquid interface of liquid media (for reviews, please see references 14 and 15). Biofilm formation consists of distinct stages encompassing reversible to irreversible attachment, microcolony formation, and maturation. Although these steps are relatively conserved for many bacterial species (for reviews, please see references 6, 16, 17, and 18), factors required for bacterial biofilm formation vary, depending on the growth conditions and environments (19, 20), and their spatial organization remains largely unexplored. During growth in yeast extract-Casamino Acids (YESCA) medium, uropathogenic *E. coli* (UPEC) cells form a floating pellicle biofilm that can be lifted off the broth surface (Fig. 1A). In this study, we took advantage of the robust nature of the pellicle biofilm and several imaging modalities to analyze the ultrastructure of UPEC pellicles.

We found striking differences in biofilm architecture between the air-liquid interfaces of UPEC pellicles. Sandwiched between these interfaces, bacterial communities exhibited different population densities within an organized dense fibrous network spanning the entire pellicle extracellular matrix (ECM). The biofilm phenotypes of mutants lacking curli fibers, cellulose, type 1 pili, and flagella provided further insights into fiber compositions of the various ECM substructures. Taken together, these observations demonstrate an intricate biofilm ultrastructure surrounding spatially segregated bacterial subpopulations.

## RESULTS

**ECM structural features containing distinct bacterial subpopulations are spatially distributed.** When grown in YESCA me-

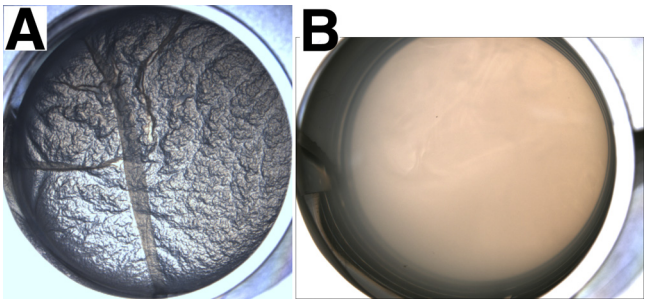


**FIG 1** UPEC cells form different types of biofilm grown in YESCA medium. When cultured in YESCA medium at 30°C, UPEC cells form curli-mediated biofilms. (A) Wild-type UTI89 forms a pellicle biofilm that exhibited the dry and wrinkled morphology. (B) In-frame deletion of the *csgA* gene abolished the formation of pellicle biofilm.

dium, the cystitis UPEC isolate UTI89 forms a pellicle biofilm (Fig. 1A) that depends on extracellular curli amyloid fiber assembly (Fig. 1B). Although curli are presumed to be required for cell-to-cell contacts, their localization within the pellicle biomass has not been determined. We therefore assessed the presence of curli fibers within UTI89 pellicles by Western blot analysis using antibodies that recognize the major curli subunit, CsgA. Because CsgA polymers are resistant to heat and SDS denaturation, 1,1,1,3,3,3-hexafluoro-2-propanol (HFIP) was used to liberate CsgA monomers for separation by PAGE (21). CsgA was found in HFIP-treated pellicles but not in untreated pellicles or planktonic bacteria (Fig. 2A). These observations confirmed polymerized curli fibers as a prominent pellicle biofilm constituent. We next examined the spatial distribution of curli subunit expression using confocal laser scanning microscopy (CLSM) of UTI89 expressing green fluorescent protein (GFP) from the *csgBA* promoter (UTI89 hk::*csgBA*pGFP). GFP expression was observed throughout the pellicle (Fig. 2B) but only rarely in the planktonic population (Fig. 2C). CLSM images of pellicle biofilms further revealed distinct morphological features at the air-exposed and liquid-submerged pellicle surfaces (Fig. 2B). While the air-exposed side exhibited a relatively smooth surface, the liquid-submerged side was rough with the characteristic mound-and-valley architecture similar to what is observed for abiotic surface biofilms (22). Furthermore, GFP fluorescence in the liquid-submerged side appeared to be reduced (Fig. 2B), suggestive of lower curli gene expression on the side submerged in medium.

We used various electron microscopy (EM) techniques to further investigate the pellicle architecture. In agreement with CLSM, transmission EM (TEM) and scanning EM (SEM) also revealed two morphologically distinct bacterial subpopulations. Bacteria near the air-exposed surface were covered by a unique mat-like surface structure (Fig. 3A; see Fig. S1A in the supplemental material) that appeared to be composed of densely packed fibers (Fig. 3B). Beneath the air-exposed surface, bacteria were tightly packed against each other (Fig. 3C). A dense fiber layer surrounded each bacterium with additional fiber matrices in the ECM (Fig. 3C and D). In sharp contrast with the air-exposed surface of the pellicle, bacteria on the liquid-submerged surface were rod shaped and occasionally filamentous (Fig. 4A; see Fig. S1B). TEM analysis revealed that bacteria on the liquid-submerged side of the pellicle were loosely packed and often not surrounded by a dense fiber layer (Fig. 4B). Furthermore, bacteria

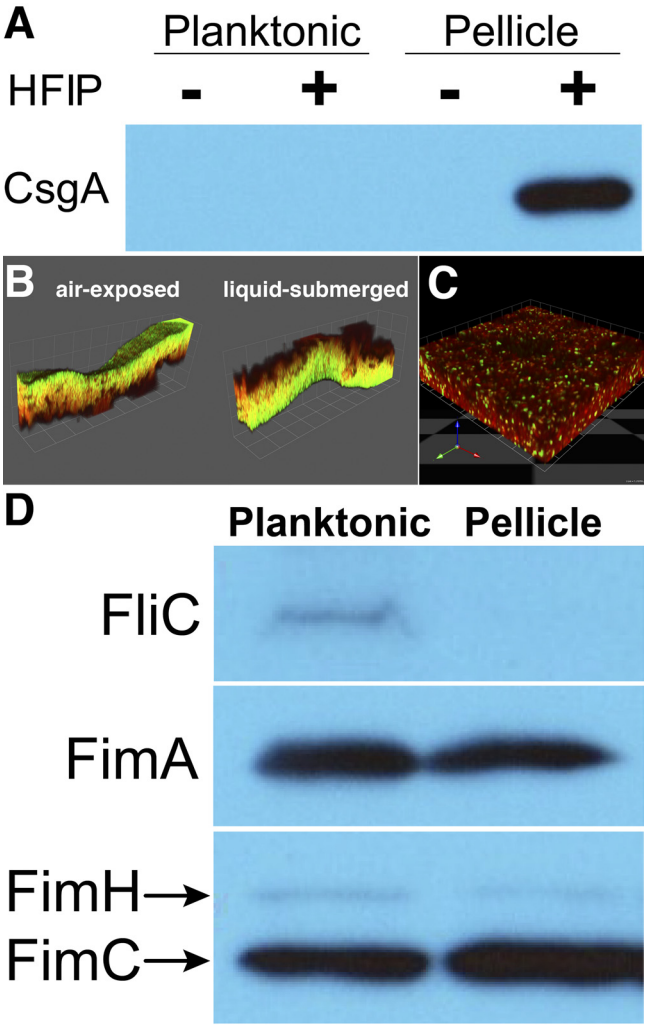


**FIG 2** Expression of extracellular organelles in pellicle versus planktonic cells. The expression of curli, type 1 pili, and flagella in 72-h-old pellicles was examined by Western blot analysis and reporter assays. (A) Western blot analysis with anti-CsgA antiserum revealed the presence of CsgA in pellicles but not in the planktonic population. SDS-insoluble CsgA was detected after HFIP treatment (+), which dissociates monomeric CsgA from curli fibers. (B and C) Three-dimensional CLSM-reconstructed images showing *csgBA* promoter-driven GFP expression in the pellicle (B) but rarely in planktonic bacterial populations (C). Two views of a pellicle are shown in panel B. On the left, the air-exposed side of the pellicle is oriented to the top, while the liquid-submerged side is at the bottom of the 3D reconstructed image. On the right, the liquid-submerged side is oriented to the top. The pellicle biofilm is 34.4 $\mu$m thick on average (range of 22.4 to 43.4 $\mu$m). The thickness of the planktonic bacterium image is due to the large number of bacteria spotted on the microscope slide, not actual biofilm. (D) Western blot analysis probing FliC, FimA, and FimCH expression in pellicles and planktonic bacteria. Unit grid size: panel B, 14.2 $\mu$m; panel C, 7.1 $\mu$m.

surrounded by dense fiber layers often had increased space surrounding them compared to those near the air-exposed region (Fig. 4B).

Further analysis using freeze-fracture high-resolution EM revealed a highly ordered ECM with two distinct structures—fibrous casings and fiber networks. Each bacterium within the pellicle was encased by a woven fibrous material (Fig. 5A and B) that directly contacted each bacterium at small, discrete regions (Fig.

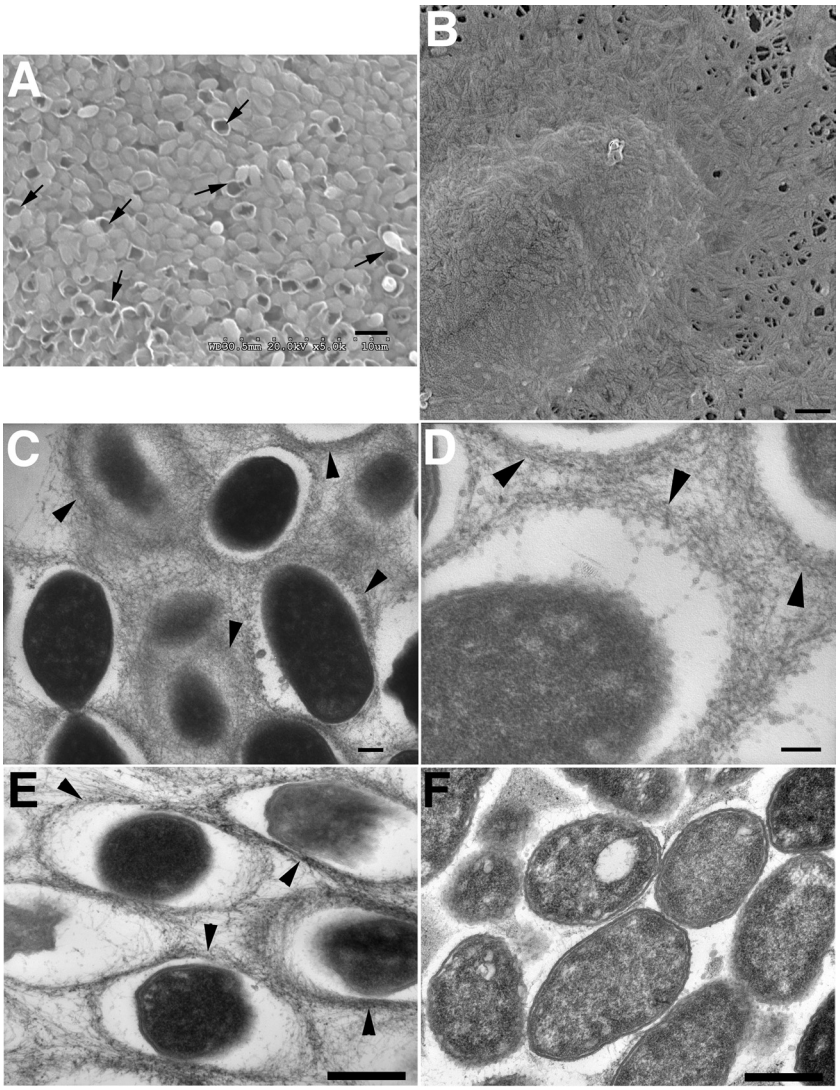


**FIG 3** Morphology and fibrous nature of the air-exposed side of pellicles and agar plate colony biofilms. (A) SEM analysis depicting the air-exposed side of UPEC pellicles. Bacteria in this area appeared to be covered by an extracellular mat. In some instances, breakage of the mat exposed hollow structures with bacterial cells nearby. A few examples of these are indicated by black arrows. (B) Quick-freeze deep-etch high-resolution EM micrographs of the air-exposed side of UPEC pellicles show the details of the mat that caps the pellicle surface. The protrusion seen in the image was due to the presence of a wt UTI89 bacterium underneath the extensive extracellular fiber covering. (C) TEM images of pellicle sections show extensive fibrous networks as the primary ECM component in the pellicle biofilm. A denser layer of fibers, as indicated by black arrowheads, immediately surrounding each bacterium also can be seen. (D) Membrane vesicles within pellicle biofilms are seen primarily within the space between bacteria and the ECM. Denser layers of fibers surrounding bacteria are also visible and indicated by black arrowheads. (E) TEM analyses of wt UTI89 agar-plate colony biofilm showed similar ECM morphology as that in pellicle biofilm. Denser layers of fibers surrounding bacteria forming fibrous casings also can be seen and are indicated by black arrowheads. (F) Deletion of the *csgA* gene resulted in a drastic reduction of organized fibers in the ECM of UTI89 Δ*csgA* colony biofilm. Amorphous electron-dense materials were still visible in the intercellular space, and a few fibers could also be seen emanating from bacteria. However, these extracellular materials did not form organized fibrous casings. Scale bars: panel A, 2 $\mu$m; panel B, 100 nm; panel C, 200 nm; panel D, 100 nm; panels E and F, 500 nm.

5C). Encased bacteria were connected indirectly to each other through extensive ECM fiber networks (Fig. 5; see Fig. S2 in the supplemental material). Using TEM, we found that this fiber network was distributed throughout the majority of the pellicle (Fig. 3C). Furthermore, the dense fiber layer immediately surrounding each bacterium seen by TEM (Fig. 3C and D) corresponds to the fibrous casing observed by freeze-fracture high-resolution EM (Fig. 5). Both TEM and freeze-fracture high-resolution EM also revealed the presence of membrane vesicles, which were primarily found in the space between bacteria and their fibrous casings (Fig. 3D; see Fig. S3 in the supplemental material).

We hypothesized that curli fibers are a major component of both the fibrous bacterial casings and the fibrous ECM matrix. Because the curli-deficient mutant (UTI89 Δ*csgA*) was unable to form pellicles, we examined mutant and wild-type (wt) bacterial colony biofilms from YESCA plates to determine whether curli fibers affect ECM structures. YESCA plate colony biofilms exhibit a wrinkled, curli-dependent morphology that resembles the air-exposed pellicle surface (see Fig. S4A in the supplemental material). Furthermore, both types of biofilms are exposed to a dehydration condition of air-exposed surface on one side and have access to the nutritional contents of YESCA medium on the other. TEM images of wt UTI89 plate colony biofilm showed morphological features similar to those in pellicle ECM, specifically a fibrous matrix in the ECM and dense, fibrous casings surrounding individual bacteria (Fig. 3E; see Fig. S4B). TEM analysis of the colony biomass formed by the curli-deficient UTI89 Δ*csgA* mutant was notable for an absent fibrous matrix and absent fibrous casings (Fig. 3F; see Fig. S4C), supporting a major role for curli in constructing or stabilizing these features. Taken together, the EM studies revealed that pellicle bacteria were nestled in fibrous casings that were, in turn, surrounded by a highly ordered fibrous ECM network bordered by distinct air-liquid interface ultrastructures. Moreover, our study suggested that curli were also likely a major constituent of the fibrous casings and ECM network in the pellicles.

**Factors contributing to pellicle biofilm ultrastructure and stability.** Although curli fibers are essential for UPEC pellicle formation, and their absence abolishes pellicle entirely (23) (Fig. 1B), they are not sufficient for robust pellicle formation. Previous reports identified cellulose, type 1 pili, and flagella as contributing factors (19, 23, 24). The absence of these factors significantly influences but does not abolish pellicle formation. We took advantage of mutants lacking these components to (i) ascertain their contributions to pellicle infrastructure and (ii) gain insights into ECM composition.

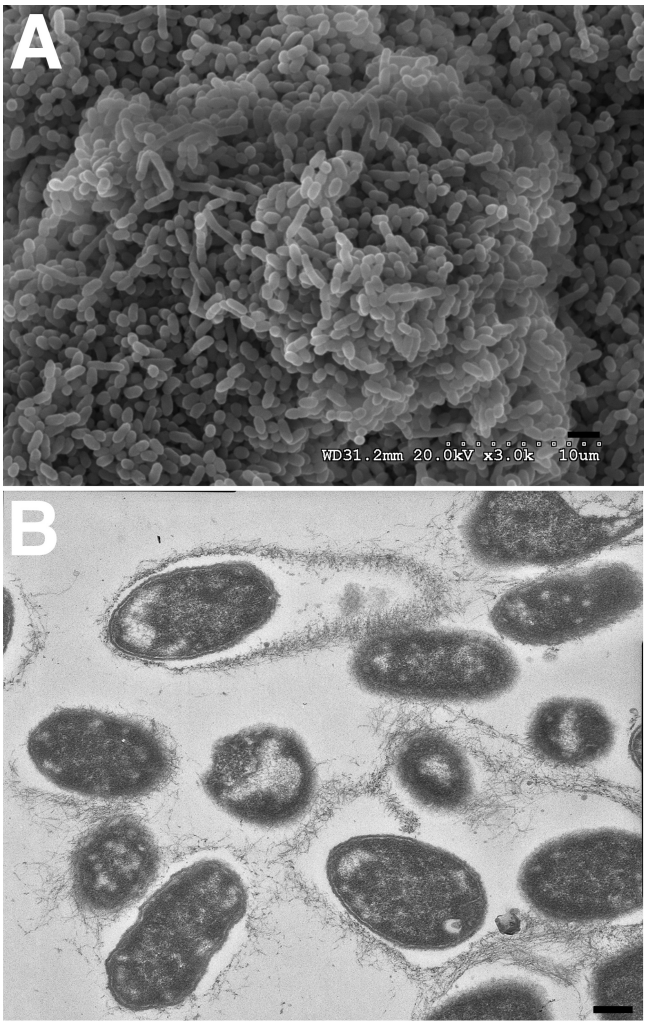


**FIG 4** Morphology of the liquid-submerged side of pellicles. (A) SEM and (B) TEM images of the liquid-submerged side of pellicles. Scale bars: panel A, 2 $\mu$m; panel B, 100 nm.

**Cellulose.** To study the contribution of cellulose, we interrogated the ability of a cellulose-deficient mutant, UTI89 Δ*yhjO*, to form pellicles. The UTI89 Δ*yhjO* pellicle was significantly weakened, could not support its own biomass, and partially collapsed during culturing (Fig. 6A). Quick-freeze deep-etch high-resolution EM of the air-exposed surface of UTI89 Δ*yhjO* pellicles revealed that bacteria were still encased in fibrous structures (Fig. 6B), although the casings appeared more loosely woven than those in wt UTI89 pellicles (Fig. 5B). In addition, the normally dense fiber mat covering the air-exposed surface of the pellicle appeared sparser in this region (Fig. 6C). These observations supported a role for cellulose in these structures. The presence of cellulose polymers within wt UTI89 pellicles was determined by combining base hydrolysis of the pellicle and cellulase digestion of remaining fibers with stable isotope dilution electron ionization gas chromatography-mass spectrometry (EI-GC-MS) analysis of the resulting D-glucose monomers. Because fragile UTI89 Δ*yhjO* pellicles could not be separated from planktonic cells, pellets from whole UTI89 Δ*yhjO* pellicle cultures were compared to similar preparations from wt UTI89. Relative to UTI89, the cellulose content of UTI89 Δ*yhjO* cultures was substantially reduced (Fig. 6D). The cellulose content of UTI89 was associated with the pellicle and not the planktonic fraction of YESCA cultures (see Fig. S5 in the supplemental material), indicating the presence of cellulose in the pellicle ECM and consistent with a role for cellulose in pellicle mechanical integrity.

**Type 1 pili.** Previous reports identified type 1 pili as factors contributing to YESCA pellicle formation by UPEC (19). Western blot analysis confirmed the presence of type 1 pili within pellicles and planktonic bacteria (Fig. 2D). Numerous studies have highlighted the role of the type 1 pilus tip adhesin FimH in mediating attachment to biotic and abiotic surfaces (25–27). We investigated the contribution of type 1 pili and the adhesin FimH in robust pellicle formation. Wild-type UTI89 forms pellicles by 48 h (Fig. 7A) that were macroscopically indistinguishable from the 72-h pellicles (Fig. 1A). In contrast, the *fimH* deletion mutant, UTI89 Δ*fimH*, was severely defective in pellicle formation, with only a thin layer of pellicle visible by 48 h (Fig. 7B). However,

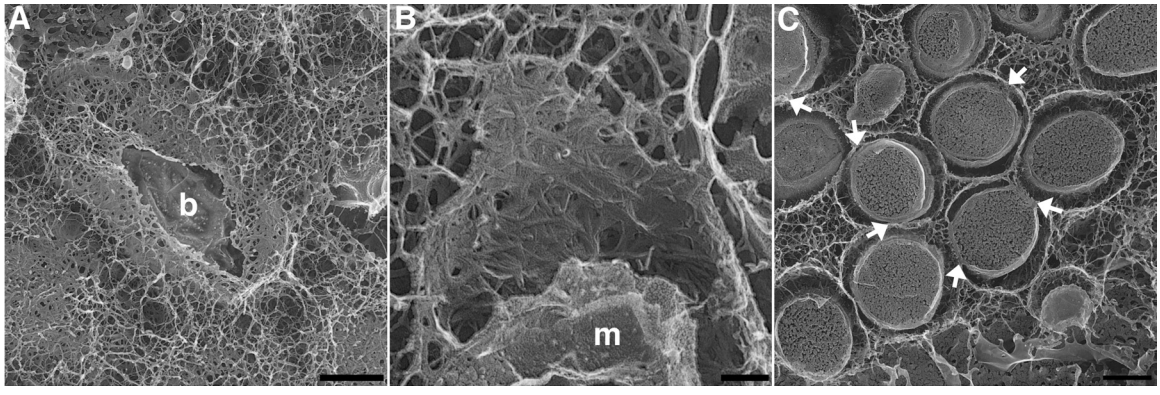


**FIG 5** Fibrous baskets encase bacteria in pellicles. Quick-freeze deep-etch high-resolution EM combined with freeze-fracture was utilized to examine the morphology of the extracellular matrix (ECM) in the pellicles. (A) Wild-type UTI89 pellicle was frozen and fractured using the sapphire disc quick-freeze method to reveal the ECM inside the pellicle. Depicted is a platinum replica of the prepared sample. A bacterium (b) is shown nestling inside a fibrous casing structure. (B) Freeze-fracture high-resolution EM analysis of pellicle revealed that the fibrous casing surrounding each bacterium was tightly woven together with fibers that eventually extended into the ECM. A portion of the residual bacterial membrane (m) remained postfracturing and is visible in the fibrous casing. (C) The freeze-fracture high-resolution EM micrograph shows that the fibrous casing surrounding pellicle bacteria came in contact with bacteria at discrete locations (white arrows). Scale bars: panel A, 500 nm; panel B, 100 nm; panel C, 500 nm.

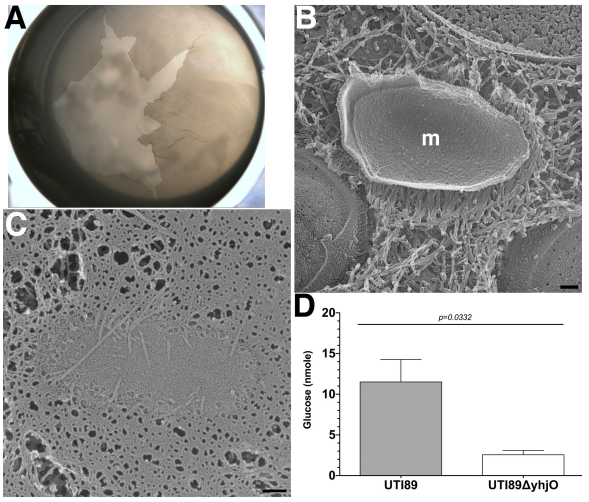


**FIG 6** Cellulose confers structural strength to pellicles. (A) Macroscopic image of a 72-h UTI89 Δ*yhjO* pellicle showing portions of the pellicle fallen to the bottom of the well. (B) Freeze-fracture high-resolution EM of UTI89 Δ*yhjO* pellicles also revealed the similar fibrous nature of the ECM and the casing surrounding each bacterium. However, in the absence of cellulose, the levels of fibers within the ECM and the casing were reduced. A portion of the residual bacterial membrane (m), including both the inner and the outer membranes, is visible in this image. (C) Cellulose was a major component of the surface mat. Quick-freeze deep-etch high-resolution EM revealed that the air-exposed surface of UTI89 Δ*yhjO* pellicle exhibited a less complex fibrous network. (D) The pellicle biofilm cultures were analyzed by EI-GC-MS for the presence of cellulose. Quantitative comparisons of the entire pellicle biofilm cultures (both pellicle and planktonic populations together) of wt UTI89 (gray bar) and the cellulose synthase mutant UTI89 Δ*yhjO* (white bar) showed a significant reduction of glucose levels derived from the mutant pellicle cultures ($P = 0.0332$). Results were derived from three separate pellicle cultures from two independent experiments. Scale bars: panels B and C, 100 nm.

UTI89 Δ*fimH* pellicles became more visible by 72 h postinoculation, although still not to the extent seen with wt UTI89 (data not shown). Addition of 2% (wt/vol) methyl-α-D-mannopyranoside into pellicle cultures, a concentration that completely inhibits mannose binding by FimH, also severely attenuated the ability of wt UTI89 to form pellicles (see Fig. S6A in the supplemental material). CLSM analysis of UTI89 Δ*fimH* pellicles revealed substantial breakage in the biofilms as well as reduced thickness compared to that of wt UTI89 (Fig. 7C; see Fig. S6B and S7A in the supplemental material). In order to determine the contribution of FimH-mediated adhesion, in addition to the presence of type 1 pilus rods, to pellicle formation, we assessed the pellicle phenotypes of an *fimH*-null mutant complemented with different FimH variants of different mannose-binding capabilities. Chromosomal complementation of UTI89 Δ*fimH* with the wild-type *fimH* gene (UTI89 wt *fimH*) restored pellicle formation to that seen with wt UTI89 (Fig. 7D; see Fig. S6C and S7B). Two FimH variants, Q133K and A62S, restored the type 1 piliation level to 50% of the wt FimH level, while the A27V V163A variant was able to fully restore type 1 piliation similar to that of wt FimH (27). Complementation with a nonfunctional FimH (UTI89 Q133K) that also resulted in decreased expression of type 1 pilus rods gave rise to thinner and weaker pellicles with visible breakage, as seen by CLSM (Fig. 7E; see Fig. S6D and S7B). Complementation of UTI89 Δ*fimH* with a low-mannose-binding-affinity FimH allele (UTI89 S62A) only partially restored the pellicle biofilm—the pel-

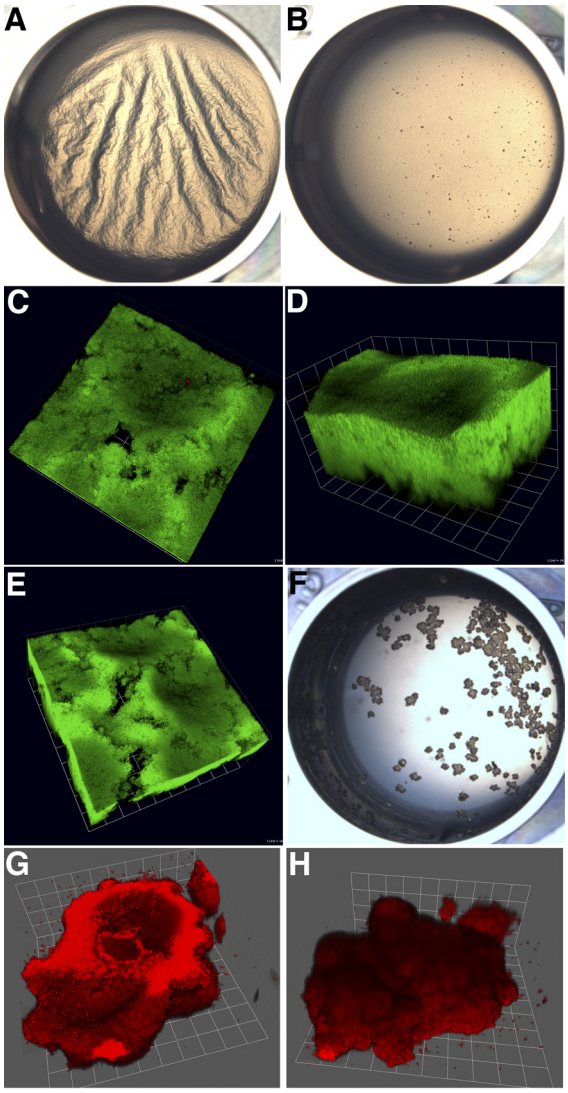


**FIG 7** Type 1 pili and flagella also play important roles on pellicle integrity or formation. (A to E) Type 1 pili play a role in the integrity of pellicles. Macroscopic images of 48-h-old pellicles showed that, unlike wt UTI89 (A), UTI89 Δ*fimH* (B) pellicle formation was compromised and the pellicle appeared thinner. The UTI89 Δ*fimH* pellicle also did not exhibit the typical wrinkled morphology. (C) Three-dimensional reconstructed CLSM images revealed extensive breakage in the 72-h-old pellicle of UTI89 Δ*fimH*. UTI89 Δ*fimH* pellicle biofilm is about 18 μm thick on average (range of 9.1 to 25.2 μm). (D and E) Genetic complementation of UTI89 Δ*fimH* with different *fimH* alleles resulted in variable phenotypes. Complementation of UTI89 Δ*fimH* with wild-type *fimH* (D) restored the pellicle biofilm to the wild-type level, in contrast to that complemented with a nonfunctional *fimH* mutant, UTI89 Q133K (E). UTI89 wt *fimH* pellicle biofilm is about 44.1 μm thick on average (range of 36.4 to 65.1 μm). UTI89 Q133K exhibited extensive breakage in the pellicle and was about 27.3 μm thick on average (range of 16.8 to 36.4 μm). (F to H) Flagella are also critical in pellicle formation. (F) Macroscopic images of pellicle cultures showed that the flagellin major subunit gene mutant, UTI89 Δ*fliC*, had a severe defect in pellicle formation. Mutants were only able to form rosette-like bacterial communities. (G and H) Three-dimensional reconstructed CLSM images showed that the UTI89 Δ*fliC* mutant rosettes retained complex biofilm morphology. The air-exposed side appeared flat or concave (G), while the liquid-submerged side exhibited mounds and valley structures similar to those of wild-type pellicles (H). The rosette biofilm thickness is about 49.3 μm on average (range of 34.7 to 63.7). The rosette biofilms of UTI89 Δ*flhDC* were indistinguishable from that of UTI89 Δ*fliC* by CLSM and thus are not presented. Unit grid size: panels C to E, 14.3 μm; panels G and H, 20.3 μm.

licles still exhibited breakages and were thinner than UTI89 wt *fimH* pellicles (see Fig. S6E and S7B). On the other hand, complementation of UTI89 Δ*fimH* with an FimH variant (UTI89 A27V V163A) that retained wild-type FimH mannose-binding ability also restored pellicle integrity to the level of UTI89 wt *fimH* (see Fig. S6F and S7B). These results demonstrated that both the intact type 1 pili and the mannose-binding ability of FimH play important roles in mediating and/or maintaining pellicle integrity.

**Flagella.** Western blot analysis detected the presence of the major flagellin subunit, FliC, only in planktonic bacteria (Fig. 2D). However, consistent with previous observations showing the contribution of flagella in biofilm formation (19), in-frame *fliC* and *flhDC* (master motility regulator) deletion mutants were also severely attenuated in their ability to form pellicles. UTI89 Δ*fliC* and UTI89 Δ*flhDC* formed small floating rosette biofilms (Fig. 7F and Fig. S6F, respectively). Although UTI89 Δ*fliC* and UTI89 Δ*flhDC* lack noticeable growth defects (19, 28, 29), they form sparse, small floating rosette biofilms (Fig. 7F; see Fig. S6G), as previously described (19). Analysis of the rosettes indicated that they were often thicker (average of 49.3 $\mu$m) than the wt UTI89 pellicles (average of 34.4 $\mu$m) (see Fig. S7A in the supplemental material). When imaged by CLSM, the rosette appeared to retain the mound-and-valley architectural features on the liquid-submerged side of the biomass, similar to those observed in wt UTI89 pellicles, while no consistent morphology was seen with the air-exposed side (Fig. 7G and H). These results strongly implicate the importance of flagella in UPEC pellicle formation, likely earlier during development, given the absence of flagella from pellicles (Fig. 2D). Collectively, our study demonstrated that the ECM of UPEC pellicle biofilms is a highly organized and complex structure comprised in part by curli and cellulose that exhibit differential spatial distributions, with type 1 pili and flagella also contributing to pellicle formation and/or integrity.

## DISCUSSION

Adaptation of free-living microorganisms to a biofilm lifestyle offers a fitness advantage during growth in hostile and nutrient-limiting environments. In this setting, collaborations and communication among bacteria within the biofilm increase community fitness (for reviews, see references 30 and 31). This is evident through increased antibiotic tolerance among bacterial biofilms. The biofilm constitutes a niche for intra- and interspecies genetic exchange, which can promote the spread of antimicrobial resistance and increased bacterial resilience (32–34). A critical component providing protection and facilitating cell-cell interactions is the presence of a self-produced extracellular matrix (ECM). Specialization in distinct ECM locations within biofilm communities contributes to biofilm resilience (35, 36).

Proteins, carbohydrates, and/or DNA have been reported to be major ECM components. The ECM has mostly been viewed as a disordered polymer array serving to hold bacteria together (1–5). In addition to ECM, biofilm resilience relies upon the unique composition of its bacterial cells. In recent years, several studies have demonstrated that biofilms are characterized by the presence of distinct subpopulations (37–40). These subpopulations may arise through genetic variation or differential expression of different genetic programs (37–41), which may be a response to a changing local environment. We captured significantly different UPEC biofilm architectures within the same biomass: microscopic analyses of pellicles revealed differences in surface morphology, bacterial population distribution, and fiber density that were most clearly related to the proximity of bacteria to the air- or liquid-exposed biofilm surfaces. The surfaces reflect two distinct exposures—harsh dehydrating conditions on the air-exposed side and a nutrient-rich niche in the liquid-submerged region. The distinct bacterial subpopulations' morphologies at these surfaces (Fig. 2B, 3, and 4) are likely responses to distinct environmental demands. DePas and colleagues (42) have reported similar bacterial subpopulations that differentially express curli and cellulose in UTI89 agar plate colony biofilms.

Employing various advanced microscopy techniques in conjunction with isogenic bacterial mutants, our study reveals a defined ECM ultrastructure that supports spatially segregated bacterial subpopulations within the pellicle biofilm. The ECM's molecular architecture was notable for a fibrous casing around each bacterium, differential surface structures, distinct spatial distributions of bacteria at pellicle surfaces, and an abundance of membrane vesicles. The fibrous casings surrounding each pellicle biofilm bacterium appear structurally complex. We speculate that bacteria expend tremendous energy in building such structures in order to protect themselves from environmental insults, such as desiccation. For example, *Salmonella* colony biofilms, which exhibit similar rough, dried, and wrinkled morphology to curli- and cellulose-producing *E. coli* colony biofilms, rely on curli and cellulose for protection against long-term dehydration and the bactericidal effects of bleach (43). Efforts are under way to investigate the biological function of the fibrous casing structures observed in the pellicles. Similarly, *Streptomyces coelicolor* and *Streptomyces lividans* cover their aerial hyphae with the amyloid-like chaplin fibers (44). It is believed that chaplins, which also form similar woven fiber patterns, protect the hyphae from dehydration, while providing structural support. The air-exposed surface of pellicles (Fig. 3B) shares morphological similarities with chaplin-coated hypha surfaces. The high-resolution EM studies we report for wt UTI89 and the UTI89 Δ*yhjO* cellulose-deficient mutant suggest that UPEC utilizes curli and cellulose fibers to create a substantial network of fibers on the air-exposed surface, which results in a mat-like structure covering the bacteria. It is likely that, similar to chaplins, curli and cellulose fibers may prevent desiccation and provided structural strength for pellicles. White and colleagues have reported that curli and cellulose fibers protected agar plate colonies of *Salmonella* spp. from desiccation and enhanced their long-term survival (43).

The abundance of membrane vesicles in the pellicles is interesting. Although their function is currently unknown, the membrane vesicles could participate in ferrying chemical messengers or bacterial components such as proteins, DNA, or carbohydrates, to allow long distance communication within the extended pellicle structure (45–49). Alternatively, the presence of membrane vesicles may be an indication of envelope stress in nearby bacteria (50). The biological consequence of these vesicles awaits additional studies.

In addition to curli fibers, other extracellular structures are also involved in robust pellicle formation. Mutations that disrupt cellulose production significantly compromised ECM architecture and impaired pellicle stability. Type 1 pili and flagella were also found to be critical in the stability and development of the biofilm substructures. Type 1 pilus-mediated adhesion was required for robust cohesion of the biomass. Motility appears critical for pellicle biofilm development, since flagella mutants are only able to

**TABLE 1** Strains used in this study

| Bacterial strain | Relevant genotype and features | Antibiotic resistance | Reference |
|---|---|---|---|
| wt UTI89 | Wild-type clinical UPEC | None | 62 |
| UTI89 hk::*csgBA*pGFP | wt UTI89 with GFP reporter under the control of curlin subunit, *csgBA*, promoter | Chloramphenicol | 23 |
| UTI89 Δ*csgA* | Deletion of the major curlin gene *csgA* in UTI89, abolishment of curli expression | None | 23 |
| UTI89 Δ*yhjO* | UTI89 *yhjO*::Cml, deletion of cellulose synthase gene *yhjO* in UTI89, abolishment of cellulose biosynthesis | Chloramphenicol | This study |
| UTI89 Δ*fimH* | UTI89 *fimH*::Kan, deletion of type 1 pilus adhesin gene *fimH* in UTI89, abolishment of FimH expression and type 1 pilus biogenesis | Kanamycin | 27 |
| UTI89 wt *fimH* | UTI89 Δ*fimH* complemented with a wild-type *fimH* on the chromosome | Kanamycin | 27 |
| UTI89 Q133K | UTI89 Δ*fimH* complemented with a nonfunctional *fimH* site-directed mutant, Q133K, on the chromosome | Kanamycin | 27 |
| UTI89 A62S | UTI89 Δ*fimH* complemented with a low-affinity *fimH* site-directed mutant, A62S, on the chromosome | Kanamycin | 27 |
| UTI89 A27V V163A | UTI89 Δ*fimH* complemented with a functional *fimH* site-directed mutant, A27V V163A, on the chromosome | Kanamycin | 27 |
| UTI89 Δ*flhDC* | UTI89 Δ*flhDC*::Kan, deletion of the dual transcriptional activators of flagellar class II operons in UTI89, abolishment of flagellar expression | Kanamycin | 29 |
| UTI89 Δ*fliC* | UTI89 Δ*fliC*::Kan, deletion of the major flagellin subunit gene *fliC* in UTI89, abolishment of flagellar expression | Kanamycin | 29 |

form sparse, small, floating rosette-like collections of bacteria (Fig. 7F; see Fig. S6G in the supplemental material). However, while flagella appear to be required for biofilm formation, they are absent in mature pellicles. This suggests a temporal regulation of biofilm factors might be facilitated by changing conditions brought on by biofilm growth. During initiation of biofilm on abiotic surfaces, flagellum-mediated mobility allows planktonic bacteria to swim to and adhere to abiotic surfaces (51–53). During pellicle biofilm formation, it is plausible that flagellum-mediated motility facilitates initial cell-to-cell interactions, allowing bacteria to form "rafts" on the air-liquid interface that seed "microcolony" formation, which eventually induces curli gene expression. Once curli are expressed, flagellum expression could decrease. There is clearly an inverse relationship between curli and flagellar gene expression (Fig. 2A and D). Furthermore, Pesavento et al. found that increased cyclic di-GMP stimulates expression of the CsgD curli transcriptional activator and represses flagellum production in a highly organized manner that involves at least two hierarchical regulatory cascades (54, 55). Here we show that flagellum-mediated motility is a prerequisite for pellicle formation and very likely precedes curli gene expression, similar to abiotic surface biofilm (56).

Extracellular DNA (eDNA) has been identified as a major ECM contributor of several types of biofilm (1–3, 5). UPEC pellicle development was not affected in the presence of 5 $\mu$g/ml DNase I (data not shown); however, at this point, we cannot entirely rule out the presence of eDNA in the ECM. Nevertheless, eDNA did not appear to play a major role in robust pellicle formation.

The assembly of bacterial extracellular structures (e.g., type 1 pili and curli), is often directed by coordinated processes involving dedicated molecular machinery (57, 58). Our observations suggest that curli and cellulose fibers secreted by biofilm bacteria are the primary components of the pellicle ECM, with type 1 pili providing additional support. Once they are on the bacterial surfaces, however, there have not been reports of further coordinated organization of these extracellular structures. Our data indicate that curli and cellulose form the fibrous mat on the top pellicle surface, matrix fibers in the ECM, and fibrous casings surrounding individual bacteria. However, the exact macromolecular interactions that lead to the formation of the observed tight matrix casings remain unclear. Interestingly, EM analyses demonstrated that the woven fibrous casings are more prominent in the regions closer to the air-exposed surface (Fig. 3C and D and Fig. 5) compared to the liquid-submerged region (Fig. 4B). Similarly, the *gfp* reporter signal associated with *csgBA* gene expression was reduced in bacteria on the pellicle's liquid-submerged surface. This observation parallels the TEM results showing lower ECM fiber density in this region and is in direct agreement with the hypothesis that curli are needed to stabilize the ECM and are repressed during planktonic growth. ECM density and composition may be affected by the local microenvironment. We cannot completely rule out the possibility that photobleaching of samples during acquisition resulted in reduced signal intensity, although we did not see an equivalent decrease of intensity in the nucleic acid dye fluorescence (red fluorescence). We are currently seeking to quantify spatial localization of curli fibers using other methodologies.

Bacterial biofilms in drinking water supplies that harbor pathogens pose potential danger to human health (59). Larsen and colleagues reported that amyloid fibers are present in the ECM of natural biofilms from many different water sources, including drinking water reservoirs (60). Understanding the molecular basis of ECM formation of an organized matrix that embeds bacteria will enhance our understanding of biofilm development. Moreover, understanding how these factors build the biofilm's ECM infrastructure may elucidate new strategies for targeting biofilm assembly and formation.

## MATERIALS AND METHODS

**Media, reagents, and bacterial strains.** A fully sequenced and well-characterized clinical UPEC isolate, UTI89, was used in this study (61, 62). All isogenic mutants of UTI89 used in this study were generated using published protocols and reagents (63, 64). These mutants and their genetic manipulations are listed in Table 1. Chromosomal *fimH*-complemented strains of UTI89 have been previously characterized and published (27). All bacterial strains were grown in Difco Luria-Bertani broth (Miller's LB) (BD, Franklin Lakes, NJ) for general culturing purposes. The general reagents used in this study, such as *N*,*O*-bis(trimethylsilyl) trifluoroacetamide (BSTFA) (Supelco, Bellefonte, PA), trimethylchlorosilane (TMCS) (Sigma, St. Louis, MO), paraformalde-

hyde (Electron Microscopy Sciences, Hatfield, PA), glutaraldehyde (Sigma, St. Louis, MO), phosphate-buffered saline (PBS) (Sigma, St. Louis, MO), sodium hydroxide (Sigma, St. Louis, MO), *Trichoderma reesei* (ATCC 26921) cellulase (Sigma, St. Louis, MO), sodium acetate (Sigma, St. Louis, MO), 1,1,1,3,3,3-hexafluoro-2-propanol (HFIP) (Sigma, St. Louis, MO), polyvinylidene difluoride (PVDF) membrane (Millipore), Casamino Acids (BD, Franklin Lakes, NJ), and yeast extract (BD, Franklin Lakes, NJ) are all commercially available. Rabbit anti-CsgA antisera were custom generated against purified CsgA proteins (Proteintech Group, Inc., Chicago, IL). Rabbit antisera raised against type 1 pili and FimCH complexes were custom generated against purified type 1 pili and FimCH protein complexes, respectively (Sigma Genosys, St. Louis, MO). Anti-FliC antiserum was kindly provided by Harry Mobley (65). Horseradish peroxidase (HRP)-conjugated anti-rabbit IgG secondary antibody was purchased from Sigma (St. Louis, MO). Supersignal West Dura extended-duration substrate was purchased from Thermo Scientific (Rockford, IL).

**Pellicle biofilm and YESCA agar plate colony biofilm cultures.** UPEC pellicle cultures were grown statically in YESCA medium (1% Casamino Acids and 0.12% yeast extract) in 24-well plastic plates (TPP, Switzerland). Briefly, bacteria were grown in 2 ml LB broth from single colonies for 3 to 5 h on a shaker. Subsequently, bacteria were diluted 1,000-fold into 2 ml/well YESCA medium to initiate pellicle biofilm culture. Unless specifically indicated, pellicle biofilm cultures were incubated at 30°C for 72 h statically before analyses were performed.

UPEC colony biofilms were grown on YESCA agar plates (1% Casamino Acids, 0.12% yeast extract, 2% Bacto agar) supplemented with Congo red and bromophenol blue (10 $\mu$g/ml and 3 $\mu$g/ml, respectively). Briefly, bacteria were grown in 2 ml LB broth from single colonies for 3 to 5 h on a shaker. Subsequently, 5-$\mu$l cultures were spotted onto YESCA agar plates and incubated at 30°C for 48 h before analyses were performed.

**Western blot analysis.** Bacteria from UTI89 pellicle cultures were subjected to Western blot analysis to determine the presence of bacterial proteins. Pellicle and planktonic bacterial populations from the same biofilm cultures were harvested separately after 72 h of static growth. Bacteria in the pellicles were mechanically separated with a hand-held homogenizer by brief homogenization for 20 s to ensure separation but viability of bacteria. Cell densities of both homogenized pellicle and planktonic populations were normalized to an optical density at 600 nm of 1. For each Western blot analysis, 150 $\mu$l of normalized bacterial suspension was processed further according to the protein of interest. Western blot analysis of CsgA was performed as previously described (66). Briefly, bacterial pellets from the pellicle or planktonic culture were treated with or without 70 $\mu$l HFIP to depolymerize curli fibers. HFIP-treated samples were then dried in a Speedvac at 45°C for 35 min and resuspended in 150 $\mu$l 2× SDS loading buffer. Bacterial pellets not treated with HFIP were resuspended directly in 150 $\mu$l 2× SDS loading buffer. Non-HFIP-treated samples were also used for detection of FliC. For Western analysis of type 1 pili, bacterial lysates in 150 $\mu$l SDS loading dye were acidified with 3 $\mu$l 1 M HCl, boiled for 5 min, and then neutralized with 3 $\mu$l 1 M NaOH (29). Seven microliters of each sample was resolved on 15% SDS-PAGE gels. Subsequent to electrophoresis, proteins were transferred to polyvinylidene difluoride (PVDF) membranes using a semidry blotting apparatus (Fisher Biotech, Fisher Scientific, Pittsburgh, PA) at 10 V for 20 min. Blots were probed with primary antisera (against either CsgA, FimA, FimCH complex, or FliC) followed by horseradish peroxidase (HRP)-conjugated goat anti-rabbit secondary antibodies.

**Cellulose determination.** Cellulose in the pellicle cultures was determined and quantified either separately from pellicle and planktonic populations within the same culture or together as a whole. In either case, bacteria and/or pellicles were pelleted and hydrolyzed with 0.1 M sodium hydroxide at 60°C for 4 h to solubilize noncellulose components and to enrich for cellulose-like polymers containing base-resistant $\beta$(1-4)-linked D-glucose subunits. The remaining solid material was washed multiple times with water to remove solubilized material before digestion with cellulase to release cellulose-bound $\alpha$- and $\beta$-D-glucose monomers. Cellulase was dissolved in 50 mM sodium acetate (pH 5.0) to the final concentration of 2.1 U/ml. Cellulase digestion (total volume of 500 $\mu$l) proceeded to completion by 6 h at 37°C with constant agitation. The presence of glucose monomers released from cellulose in the pellicles was determined via electron ionization gas chromatography-mass spectroscopy (EI-GC-MS). [$^{13}C_6$]glucose internal standard was first added to 100 $\mu$l of hydrolyzed supernatant to a final concentration of 0.5 mM. The mixture was further derivatized with 100 $\mu$l BSTFA plus 10% TMCS and analyzed by EI-GC-MS with ion monitoring at 435, 393, and 204 *m*/*z* for unlabeled glucose and 441, 397, and 206 *m*/*z* for the internal standard. To quantify cellulose levels, samples were compared to a glucose standard curve using D-glucose derivatized in the same manner.

**Confocal laser scanning microscopy, 3D reconstruction, and biofilm thickness measurements.** Pellicle biofilms were first fixed in 3.5% paraformaldehyde in PBS for 30 min followed by several successive rinsing with PBS. Fixed biofilms were subsequently stained with 5 $\mu$M orange fluorescent nucleic acid dye SYTO83 or SYTO9 (Invitrogen, Carlsbad, CA) for 15 min. Biofilms were washed again with PBS several times after staining to remove excess dye and mounted on microscope slides with Prolong antifade gold (Invitrogen, Carlsbad, CA). Pellicle biofilms were examined on an LSM 510 Meta laser scanning confocal microscope (Carl Zeiss, Thornwood, NY) with a 63× oil immersion objective. Optical section images were acquired with LSM Image Examiner (Carl Zeiss, Thornwood, NY). Three-dimensional (3D) reconstruction of biofilm images from optical section images was performed with Volocity software (Improvision, Inc., Waltham, WA). The thickness of pellicle biofilms or rosettes was measured from the xz plane of 3D reconstructed images with Volocity software. Multiple measurements were taken within the same plane and from multiple samples.

Planktonic bacteria were analyzed in a similar manner. One milliliter of planktonic culture was pelleted, resuspended in 50 $\mu$l PBS, and then fixed and stained following the same protocol for pellicle biofilms. After final rinsing, bacteria were pelleted again and resuspended in 10 $\mu$l PBS. Two microliters of bacterial suspension was spotted onto a microscope slide and air-dried before samples were mounted with Prolong antifade gold and a coverslip. CLSM image acquisition and processing were performed according to the same protocol as for pellicle biofilms.

**Thin-section TEM.** For ultrastructural analyses, thin-section transmission electron microscopy (TEM) was employed. Pellicles were fixed in 2% paraformaldehyde–2.5% glutaraldehyde (Polysciences Inc., Warrington, PA) in PBS (pH 7.4) for 1 h at room temperature. Samples were then embedded in 2% low-melt agarose, washed in PBS, and postfixed in 1% osmium tetroxide (Polysciences, Inc., Warrington, PA) for 1 h. Bacterial colonies were first embedded in agarose before fixation with paraformaldehyde and glutaraldehyde, as described above. Embedded and fixed bacterial colonies were then postfixed with osmium tetroxide, also as described above. Subsequently, samples were rinsed extensively in distilled water ($dH_2O$) prior to *en bloc* staining with 1% aqueous uranyl acetate (Ted Pella, Inc., Redding, CA) for 1 h. Following several rinses in $dH_2O$, samples were dehydrated in a graded series of ethanol and embedded in Eponate 12 resin (Ted Pella, Inc.). Sections of 95 nm were cut with a Leica Ultracut UCT ultramicrotome (Leica Microsystems, Inc., Bannockburn, IL), stained with uranyl acetate and lead citrate, and viewed on a JEOL 1200 EX transmission electron microscope (JEOL USA, Inc., Peabody, MA).

**SEM.** For scanning electron microscopy (SEM), pellicle biofilms were fixed in 4% paraformaldehyde–2.5% glutaraldehyde in 0.1 M cacodylate for 1 h at room temperature (26°C). After several rinses with 0.1 M cacodylate, fixed pellicles were prepared for SEM visualization according to a published protocol (67).

**Quick-freeze deep-etch, "sapphire disc" quick-freeze, and freeze-fracture high-resolution EM.** Quick-freeze deep-etch EM was performed according to published protocols, with minor modifications (68). Pieces of pellicle biofilms, either manually torn in the case of wt UTI89 or natu-

rally broken in the case of UTI89 Δ*yhjO*, were transferred from culture wells to float on top of culture dishes containing NaHCa solution (100 mM NaCl, 30 mM HEPES, 2 mM $CaCl_2$). Pellicles were then picked up from underneath onto small 3- by 3-mm pieces of glass coverslip and quick-frozen by forceful impact against a pure copper block cooled to 4 K with liquid helium. Frozen pellicles were then mounted in a Balzers 400 vacuum evaporator, at which point they were warmed to −100°C, freeze-fractured, "deep-etched" by vacuum sublimation for 3 min, and then rotary replicated with ~3 nm of platinum deposited from an electron beam gun mounted at 15° above the horizontal. Immediately thereafter, a stabilizing film of ~10 nm of pure carbon was deposited onto the replica from an 85° angle. Replicas were floated off the glass onto a dish containing concentrated hydrofluoric acid. The released replicas were further cleaned by transfer through successive 10-ml petri dishes of the following solutions, each containing a loopful of Photo-flo, for the given times: $dH_2O$, 5 min; household bleach, 20 min, with 2 exchanges of $dH_2O$ at 5 min per exchange. Finally, replicas were picked up on Formvar-coated 400 mesh copper grids, viewed in a JEOL 100CX microscope, and photographed with an AMT digital camera.

"Sapphire disc" fracturing was performed similarly, with minor modifications. Briefly, after pellicles were picked up on a piece of glass coverslip, a 3-mm-diameter disk of pure sapphire, 0.05 mm thick, was laid on top of the pellicle, sandwiching the biofilm in between, and the whole sandwich was again quick-frozen by forceful impact of the sapphire disk against the copper block cooled to 4 K. Fracturing was then achieved by "popping" the sapphire disk off of the frozen sample, using the $LN_2$-cooled microtome knife as a lever. The sample subsequently underwent the same deep-etching and replication processes described above.

**Statistical analysis.** Statistical analyses were performed with Prism software (GraphPad Software, Inc., La Jolla, CA). Unpaired Student's *t* test was performed. The two-tailed *P* values are presented.

## SUPPLEMENTAL MATERIAL

Supplemental material for this article may be found at http://mbio.asm.org/lookup/suppl/doi:10.1128/mBio.00645-13/-/DCSupplemental.

Figure S1, JPG file, 2.1 MB.
Figure S2, JPG file, 2.7 MB.
Figure S3, JPG file, 2.3 MB.
Figure S4, JPG file, 2.5 MB.
Figure S5, TIF file, 2.2 MB.
Figure S6, JPG file, 1.9 MB.
Figure S7, JPG file, 2 MB.

## ACKNOWLEDGMENTS

We thank Swaine Chen and Corinne Cusumano for helpful discussions. We are grateful for the excellent technical assistance with TEM from Wandy Beatty and Ling Lu at the Molecular Microbiology Imaging Facility, with SEM from Howard Wynder at the Histology and Microscopy Core Facility and Jaclynn Lett at the Microscopy and Digital Imaging Core, and with high-resolution electron microscopy from Robyn Roth in the Department of Cell Biology and Physiology, Washington University in St. Louis. We also would like to acknowledge Jen Walker for technical assistance.

The Microscopy and Digital Imaging Core is located in the Research Center for Auditory and Visual Studies, Department of Otolaryngology, and is funded by NIH P30 DC004665. EI-GC-MS studies were supported by NIH grants RR00954, DK20579, and DK5634. In addition, this work is supported by a Career Award for Medical Scientists from the Burroughs Wellcome Fund (J.P.H.) and NIH grants K12 HD001459-09 (J.P.H.), NIH UL1 RR024992 (J.P.H.), NIH RO1 A1073847 (M.R.C.), and NIH RO1 AI048689 (S.J.H.).

## REFERENCES

1. **Steinberger RE, Holden PA.** 2005. Extracellular DNA in single- and multiple-species unsaturated biofilms. Appl. Environ. Microbiol. **71:**5404–5410.
2. **Izano EA, Amarante MA, Kher WB, Kaplan JB.** 2008. Differential roles of poly-N-acetylglucosamine surface polysaccharide and extracellular DNA in Staphylococcus aureus and Staphylococcus epidermidis biofilms. Appl. Environ. Microbiol. **74:**470–476.
3. **Qin Z, Ou Y, Yang L, Zhu Y, Tolker-Nielsen T, Molin S, Qu D.** 2007. Role of autolysin-mediated DNA release in biofilm formation of Staphylococcus epidermidis. Microbiology **153:**2083–2092.
4. **Jonas K, Tomenius H, Kader A, Normark S, Römling U, Belova LM, Melefors O.** 2007. Roles of curli, cellulose and BapA in Salmonella biofilm morphology studied by atomic force microscopy. BMC Microbiol. **7:**70. doi:10.1186/1471-2180-7-70.
5. **Guiton PS, Hung CS, Kline KA, Roth R, Kau AL, Hayes E, Heuser J, Dodson KW, Caparon MG, Hultgren SJ.** 2009. Contribution of autolysin and sortase A during Enterococcus faecalis DNA-dependent biofilm development. Infect. Immun. **77:**3626–3638.
6. **Kostakioti M, Hadjifrangiskou M, Hultgren SJ.** 2013. Bacterial biofilms: development, dispersal, and therapeutic strategies in the dawn of the postantibiotic era. Cold Spring Harb. Perspect. Med. **3:**a010306. doi:10.1101/cshperspect.a010306.
7. **Elasri MO, Miller RV.** 1999. Study of the response of a biofilm bacterial community to UV radiation. Appl. Environ. Microbiol. **65:**2025–2031.
8. **Hansen LT, Vogel BF.** 2011. Desiccation of adhering and biofilm listeria monocytogenes on stainless steel: survival and transfer to salmon products. Int. J. Food Microbiol. **146:**88–93.
9. **Kadouri D, O'Toole GA.** 2005. Susceptibility of biofilms to Bdellovibrio bacteriovorus attack. Appl. Environ. Microbiol. **71:**4044–4051.
10. **Matz C, Webb JS, Schupp PJ, Phang SY, Penesyan A, Egan S, Steinberg P, Kjelleberg S.** 2008. Marine biofilm bacteria evade eukaryotic predation by targeted chemical defense. PLoS One **3:**e2744. doi:10.1371/journal.pone.0002744.
11. **Mulcahy H, Charron-Mazenod L, Lewenza S.** 2008. Extracellular DNA chelates cations and induces antibiotic resistance in Pseudomonas aeruginosa biofilms. PLOS Pathog. **4:**e1000213. doi:10.1371/journal.ppat.1000213.
12. **Haaber J, Cohn MT, Frees D, Andersen TJ, Ingmer H.** 2012. Planktonic aggregates of Staphylococcus aureus protect against common antibiotics. PLoS One **7:**e41075. doi:10.1371/journal.pone.0041075.
13. **Roberts ME, Stewart PS.** 2005. Modelling protection from antimicrobial agents in biofilms through the formation of persister cells. Microbiology **151:**75–80.
14. **Anderson GG, Dodson KW, Hooton TM, Hultgren SJ.** 2004. Intracellular bacterial communities of uropathogenic *Escherichia coli* in urinary tract pathogenesis. Trends Microbiol. **12:**424–430.
15. **Branda SS, Vik S, Friedman L, Kolter R.** 2005. Biofilms: the matrix revisited. Trends Microbiol. **13:**20–26.
16. **Davey ME, O'Toole GA.** 2000. Microbial biofilms: from ecology to molecular genetics. Microbiol. Mol. Biol. Rev. **64:**847–867.
17. **O'Toole G, Kaplan HB, Kolter R.** 2000. Biofilm formation as microbial development. Annu. Rev. Microbiol. **54:**49–79.
18. **Vlamakis H, Chai Y, Beauregard P, Losick R, Kolter R.** 2013. Sticking together: building a biofilm the Bacillus subtilis way. Nat. Rev. Microbiol. **11:**157–168.
19. **Hadjifrangiskou M, Gu AP, Pinkner JS, Kostakioti M, Zhang EW, Greene SE, Hultgren SJ.** 2012. Transposon mutagenesis identifies uropathogenic *Escherichia coli* biofilm factors. J. Bacteriol. **194:**6195–6205.
20. **Andrews JS, Rolfe SA, Huang WE, Scholes JD, Banwart SA.** 2010. Biofilm formation in environmental bacteria is influenced by different macromolecules depending on genus and species. Environ. Microbiol. **12:**2496–2507.
21. **Zhou Y, Blanco LP, Smith DR, Chapman MR.** 2012. Bacterial amyloids. Methods Mol. Biol. **849:**303–320.
22. **Banin E, Vasil ML, Greenberg EP.** 2005. Iron and Pseudomonas aeruginosa biofilm formation. Proc. Natl. Acad. Sci. U. S. A. **102:**11076–11081.
23. **Cegelski L, Pinkner JS, Hammer ND, Cusumano CK, Hung CS, Chorell E, Aberg V, Walker JN, Seed PC, Almqvist F, Chapman MR, Hultgren SJ.** 2009. Small-molecule inhibitors target *Escherichia coli* amyloid biogenesis and biofilm formation. Nat. Chem. Biol. **5:**913–919.
24. **McCrate OA, Zhou X, Reichhardt C, Cegelski L.** 1 July 2013. Sum of the parts: composition and architecture of the bacterial extracellular matrix. J. Mol. Biol. [Epub ahead of print.] doi:10.1016/j.jmb.2013.06.022.
25. **Hung CS, Bouckaert J, Hung D, Pinkner J, Widberg C, DeFusco A, Auguste CG, Strouse R, Langermann S, Waksman G, Hultgren SJ.** 2002.

Structural basis of tropism of *Escherichia coli* to the bladder during urinary tract infection. Mol. Microbiol. **44:**903–915.
26. **Harber MJ, Mackenzie R, Asscher AW.** 1983. A rapid bioluminescence method for quantifying bacterial adhesion to polystyrene. J. Gen. Microbiol. **129:**621–632.
27. **Chen SL, Hung CS, Pinkner JS, Walker JN, Cusumano CK, Li Z, Bouckaert J, Gordon JI, Hultgren SJ.** 2009. Positive selection identifies an in vivo role for FimH during urinary tract infection in addition to mannose binding. Proc. Natl. Acad. Sci. U. S. A. **106:**22439–22444.
28. **Lane MC, Lockatell V, Monterosso G, Lamphier D, Weinert J, Hebel JR, Johnson DE, Mobley HL.** 2005. Role of motility in the colonization of uropathogenic *Escherichia coli* in the urinary tract. Infect. Immun. **73:**7644–7656.
29. **Wright KJ, Seed PC, Hultgren SJ.** 2005. Uropathogenic *Escherichia coli* flagella aid in efficient urinary tract colonization. Infect. Immun. **73:**7657–7668.
30. **Høiby N, Bjarnsholt T, Givskov M, Molin S, Ciofu O.** 2010. Antibiotic resistance of bacterial biofilms. Int. J. Antimicrob. Agents **35:**322–332.
31. **Anderson GG, O'Toole GA.** 2008. Innate and induced resistance mechanisms of bacterial biofilms. Curr. Top. Microbiol. Immunol. **322:**85–105.
32. **Marks LR, Reddinger RM, Hakansson AP.** 2012. High levels of genetic recombination during nasopharyngeal carriage and biofilm formation in Streptococcus pneumoniae. mBio 3(5):e00200-12. doi:10.1128/mBio.00200-12.
33. **Grande R, Di Campli E, Di Bartolomeo S, Verginelli F, Di Giulio M, Baffoni M, Bessa LJ, Cellini L.** 2012. Helicobacter pylori biofilm: a protective environment for bacterial recombination. J. Appl. Microbiol. **113:**669–676.
34. **Gillings MR, Holley MP, Stokes HW.** 2009. Evidence for dynamic exchange of qac gene cassettes between class 1 integrons and other integrons in freshwater biofilms. FEMS Microbiol. Lett. **296:**282–288.
35. **Campos JM, Zusman DR.** 1975. Regulation of development in Myxococcus xanthus: effect of 3′:5′-cyclic AMP, ADP, and nutrition. Proc. Natl. Acad. Sci. U. S. A. **72:**518–522.
36. **Dworkin M.** 1963. Nutritional regulation of morphogenesis in Myxococcus xanthus. J. Bacteriol. **86:**67–72.
37. **Hansen S, Lewis K, Vulić M.** 2008. Role of global regulators and nucleotide metabolism in antibiotic tolerance in *Escherichia coli*. Antimicrob. Agents Chemother. **52:**2718–2726.
38. **Keren I, Shah D, Spoering A, Kaldalu N, Lewis K.** 2004. Specialized persister cells and the mechanism of multidrug tolerance in *Escherichia coli*. J. Bacteriol. **186:**8172–8180.
39. **Yang L, Nilsson M, Gjermansen M, Givskov M, Tolker-Nielsen T.** 2009. Pyoverdine and PQS mediated subpopulation interactions involved in Pseudomonas aeruginosa biofilm formation. Mol. Microbiol. **74:**1380–1392.
40. **Parsek MR, Tolker-Nielsen T.** 2008. Pattern formation in Pseudomonas aeruginosa biofilms. Curr. Opin. Microbiol. **11:**560–566.
41. **Starkey M, Hickman JH, Ma L, Zhang N, De Long S, Hinz A, Palacios S, Manoil C, Kirisits MJ, Starner TD, Wozniak DJ, Harwood CS, Parsek MR.** 2009. Pseudomonas aeruginosa rugose small-colony variants have adaptations that likely promote persistence in the cystic fibrosis lung. J. Bacteriol. **191:**3492–3503.
42. **DePas WH, Hufnagel DA, Lee JS, Blanco LP, Bernstein HC, Fisher ST, James GA, Stewart PS, Chapman MR.** 2013. Iron induces bimodal population development by *Escherichia coli*. Proc. Natl. Acad. Sci. U. S. A. **110:**2629–2634.
43. **White AP, Gibson DL, Kim W, Kay WW, Surette MG.** 2006. Thin aggregative fimbriae and cellulose enhance long-term survival and persistence of Salmonella. J. Bacteriol. **188:**3219–3227.
44. **Di Berardo C, Capstick DS, Bibb MJ, Findlay KC, Buttner MJ, Elliot MA.** 2008. Function and redundancy of the chaplin cell surface proteins in aerial hypha formation, rodlet assembly, and viability in Streptomyces coelicolor. J. Bacteriol. **190:**5879–5889.
45. **Schooling SR, Hubley A, Beveridge TJ.** 2009. Interactions of DNA with biofilm-derived membrane vesicles. J. Bacteriol. **191:**4097–4102.
46. **McBroom AJ, Johnson AP, Vemulapalli S, Kuehn MJ.** 2006. Outer membrane vesicle production by *Escherichia coli* is independent of membrane instability. J. Bacteriol. **188:**5385–5392.
47. **Renelli M, Matias V, Lo RY, Beveridge TJ.** 2004. DNA-containing membrane vesicles of Pseudomonas aeruginosa PAO1 and their genetic transformation potential. Microbiology **150:**2161–2169.
48. **Allan ND, Kooi C, Sokol PA, Beveridge TJ.** 2003. Putative virulence factors are released in association with membrane vesicles from Burkholderia cepacia. Can. J. Microbiol. **49:**613–624.
49. **Horstman AL, Kuehn MJ.** 2000. Enterotoxigenic *Escherichia coli* secretes active heat-labile enterotoxin via outer membrane vesicles. J. Biol. Chem. **275:**12489–12496.
50. **McBroom AJ, Kuehn MJ.** 2007. Release of outer membrane vesicles by gram-negative bacteria is a novel envelope stress response. Mol. Microbiol. **63:**545–558.
51. **Barken KB, Pamp SJ, Yang L, Gjermansen M, Bertrand JJ, Klausen M, Givskov M, Whitchurch CB, Engel JN, Tolker-Nielsen T.** 2008. Roles of type IV pili, flagellum-mediated motility and extracellular DNA in the formation of mature multicellular structures in Pseudomonas aeruginosa biofilms. Environ. Microbiol. **10:**2331–2343.
52. **Crawford RW, Reeve KE, Gunn JS.** 2010. Flagellated but not hyperfimbriated Salmonella enterica serovar. Typhimurium attaches to and forms biofilms on cholesterol-coated surfaces. J. Bacteriol. **192:**2981–2990.
53. **Wood TK, González Barrios AF, Herzberg M, Lee J.** 2006. Motility influences biofilm architecture in *Escherichia coli*. Appl. Microbiol. Biotechnol. **72:**361–367.
54. **Ogasawara H, Yamamoto K, Ishihama A.** 2011. Role of the biofilm master regulator CsgD in cross-regulation between biofilm formation and flagellar synthesis. J. Bacteriol. **193:**2587–2597.
55. **Pesavento C, Becker G, Sommerfeldt N, Possling A, Tschowri N, Mehlis A, Hengge R.** 2008. Inverse regulatory coordination of motility and curli-mediated adhesion in *Escherichia coli*. Genes Dev. **22:**2434–2446.
56. **Pratt LA, Kolter R.** 1998. Genetic analysis of *Escherichia coli* biofilm formation: roles of flagella, motility, chemotaxis and type I pili. Mol. Microbiol. **30:**285–293.
57. **Chapman MR, Robinson LS, Pinkner JS, Roth R, Heuser J, Hammar M, Normark S, Hultgren SJ.** 2002. Role of *Escherichia coli* curli operons in directing amyloid fiber formation. Science **295:**851–855.
58. **Orndorff PE, Falkow S.** 1984. Organization and expression of genes responsible for type 1 piliation in *Escherichia coli*. J. Bacteriol. **159:**736–744.
59. **September SM, Els FA, Venter SN, Brözel VS.** 2007. Prevalence of bacterial pathogens in biofilms of drinking water distribution systems. J. Water Health **5:**219–227.
60. **Larsen P, Nielsen JL, Dueholm MS, Wetzel R, Otzen D, Nielsen PH.** 2007. Amyloid adhesins are abundant in natural biofilms. Environ. Microbiol. **9:**3077–3090.
61. **Chen SL, Hung CS, Xu J, Reigstad CS, Magrini V, Sabo A, Blasiar D, Bieri T, Meyer RR, Ozersky P, Armstrong JR, Fulton RS, Latreille JP, Spieth J, Hooton TM, Mardis ER, Hultgren SJ, Gordon JI.** 2006. Identification of genes subject to positive selection in uropathogenic strains of *Escherichia coli*: a comparative genomics approach. Proc. Natl. Acad. Sci. U. S. A. **103:**5977–5982.
62. **Mulvey MA, Schilling JD, Hultgren SJ.** 2001. Establishment of a persistent *Escherichia coli* reservoir during the acute phase of a bladder infection. Infect. Immun. **69:**4572–4579.
63. **Datsenko KA, Wanner BL.** 2000. One-step inactivation of chromosomal genes in *Escherichia coli* K-12 using PCR products. Proc. Natl. Acad. Sci. U. S. A. **97:**6640–6645.
64. **Murphy KC, Campellone KG.** 2003. Lambda Red-mediated recombinogenic engineering of enterohemorrhagic and enteropathogenic *E. coli*. BMC Mol. Biol. **4:**11. doi:10.1186/1471-2199-4-11.
65. **Simms AN, Mobley HL.** 2008. Multiple genes repress motility in uropathogenic *Escherichia coli* constitutively expressing type 1 fimbriae. J. Bacteriol. **190:**3747–3756.
66. **Weiss-Muszkat M, Shakh D, Zhou Y, Pinto R, Belausov E, Chapman MR, Sela S.** 2010. Biofilm formation by multicellular behavior *Escherichia coli* O55:H7, an atypical enteropathogenic strain. Appl. Environ. Microbiol. **76:**1545–1554.
67. **Kelley RO, Dekker RA, Bluemink JG.** 1973. Ligand-mediated osmium binding: its application in coating biological specimens for scanning electron microscopy. J. Ultrastruct. Res. **45:**254–258.
68. **Heuser J.** 1980. Three-dimensional visualization of coated vesicle formation in fibroblasts. J. Cell Biol. **84:**560–583.